

## Article

# Using Remote Sensing and GIS-Based Frequency Ratio Technique for Revealing Groundwater Prospective Areas at Wadi Al Hamdh Watershed, Saudi Arabia

Mohamed Abdekareem <sup>1,\*</sup>, Fathy Abdalla <sup>1,2</sup>, Nassir Al-Arifi <sup>3,\*</sup>, Abdullah O. Bamousa <sup>4</sup> and Farouk El-Baz <sup>5</sup>

<sup>1</sup> Geology Department, South Valley University, Qena 83523, Egypt

<sup>2</sup> Deanship of Scientific Research, King Saud University, Riyadh 68953, Saudi Arabia

<sup>3</sup> Chair of Natural Hazards and Mineral Resources, Geology and Geophysics Department, King Saud University, Riyadh 11451, Saudi Arabia

<sup>4</sup> Geology Department, Taibah University, Al Madinah Al Munawarah 42353, Saudi Arabia

<sup>5</sup> Center for Remote Sensing, Boston University, Boston, MA 02215, USA

\* Correspondence: mohamed.abdelkareem@sci.svu.edu.eg (M.A.); nalarifi@ksu.edu.sa (N.A.-A.)

**Abstract:** For socioeconomic development in arid regions, there is an increasing need for groundwater resources due to rapid population expansion. It is necessary to apply innovative approaches for managing the sustainability of groundwater resources. Thus, remote sensing, geologic, climatic, and hydrologic data are integrated through the GIS-based frequency ratio and overlay analysis for assessing the spatial distribution of groundwater potential zones (GWPZs) of Wadi Al Hamdh, Saudi Arabia. Twelve factors controlling groundwater's existence and infiltration were identified, normalized using the frequency ratio technique and combined through GIS techniques. To accomplish this, 313 well locations in the study area were used for training (70%) and 137 well locations were utilized for validation (30%). Using receiver operating characteristic (ROC) curves and field data, the model predictions were validated and showed very good performance (AUC: 0.893). The five zones on the GWPZs map correspond to 2.24, 5.81, 13.39, 53.90, and 24.65% of the entire area. These are: excellent, good, moderate, low, and very low perspectivity. As a good example, the applied approaches provided very good results that are significant to planning and sustainable development as well as managing groundwater resources in arid regions.

**Keywords:** modeling; groundwater; GIS; remote sensing; Al Madinah; Wadi Al Hamdh



**Citation:** Abdekareem, M.; Abdalla, F.; Al-Arifi, N.; Bamousa, A.O.; El-Baz, F. Using Remote Sensing and GIS-Based Frequency Ratio Technique for Revealing Groundwater Prospective Areas at Wadi Al Hamdh Watershed, Saudi Arabia. *Water* **2023**, *15*, 1154. <https://doi.org/10.3390/w15061154>

Academic Editor: Craig Allan

Received: 15 February 2023

Revised: 5 March 2023

Accepted: 8 March 2023

Published: 16 March 2023



**Copyright:** © 2023 by the authors. Licensee MDPI, Basel, Switzerland. This article is an open access article distributed under the terms and conditions of the Creative Commons Attribution (CC BY) license (<https://creativecommons.org/licenses/by/4.0/>).

## 1. Introduction

More than two billion people worldwide suffer from limited access to fresh water, according to The United Nations World Water Development Report [1]. By around 2050, over one-third of the global population would suffer a significant water crisis if the present level of water contamination and use are still not lowered [1]. Surface water supply systems have been facing difficulties due to rapid urbanization, a growing population, ecological pollution, and factors such as climate change and water insufficiency [2]. Such surface freshwater represents less than 1% of the world's freshwater in lakes and rivers, while over 30% of it is preserved underground as aquifers [3]. Freshwater supplies are under great stress everywhere in the globe, particularly in emerging nations [4,5].

In dry and semi-arid areas, groundwater represents the most valuable natural resource. The supply of groundwater contributes roughly 50% of the water used for potable use, 40% for industry, and 20% for agriculture [6]. As compared to surface water, groundwater is less exposed to contamination and evapotranspiration. Groundwater can also be drawn during any part of the year, and unexpected droughts have a lower effect [7–9]. Due to the over exploitation of groundwater, its levels are decreasing. Daily losses are being recorded in the underground water supply [10]. For the best use and preservation of this

priceless commodity, it is crucial to identify groundwater potential areas [11]. Drilling and geoelectric monitoring are two conventional techniques for finding groundwater; they are exceedingly time-consuming and expensive. Recent techniques can estimate the groundwater potential depending on the watershed's characteristics, and the data they produce are more reliable [12–14].

Wadi Al Hamdh, as a part of arid-semi arid regions in the west of the Arabian Peninsula, was chosen in the present study due to its significant area (108,457 sq km) that catches rainfall, location (east of the Red Sea), extension mainly through at five territories (e.g., Al Madinah, Makkah, Riyadh, Ha'il, and Tabuk), and prominent climatic and hydrologic conditions in Saudi Arabia (Figure 1).

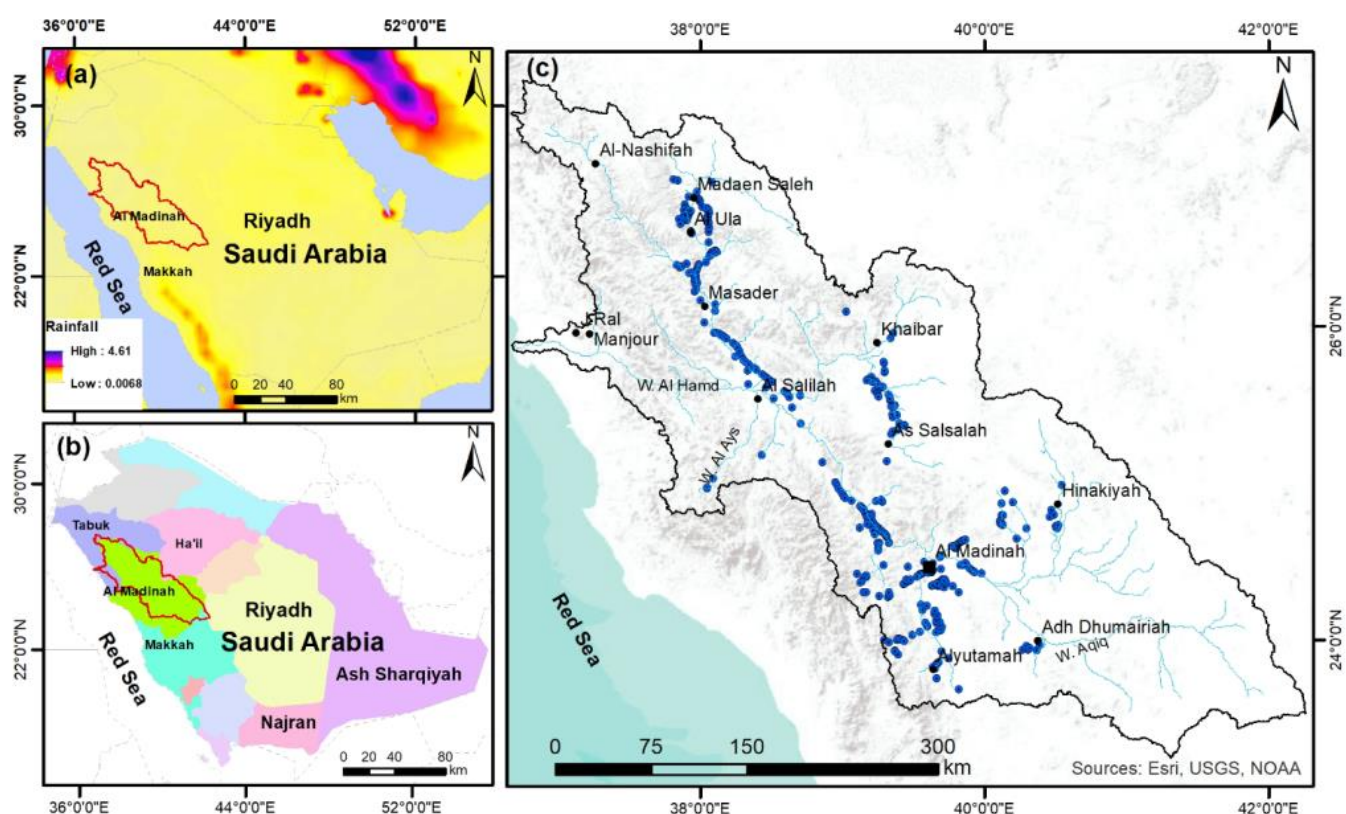


**Figure 1.** Location map of the Wadi Al Hamdh watershed. (a) A watershed of the study area in red overlain the Rainfall map; (b) A red polygon of the study area overlain the Saudi Administrative map; (c) Points showing farms, and wells.

Mapping groundwater resources, using remote sensing (RS) and geographic information systems (GIS), has become an increasingly popular technique [15,16]. Numerous elements, including geology, topography, climatic conditions, soil, land use, land cover, slopes, distances from rivers, and precipitation levels, have an impact on groundwater dispersion [7,17]. During the past few years, numerous scientists have employed a variety of cutting-edge analysis techniques and simulation approaches to pinpoint places with groundwater potential [7,18–20].

Frequency ratio (FR), for example, is a data-driven model that is frequently used in groundwater prospection [21]. This method improved the prediction output and was adopted for the groundwater potential zone, which helps decision-makers [22–26]. In order to assign rating (r) values to each class, the FR technique establishes the geographical linkages between the dependent variable, existing wells (spring wells, observation wells), and the independent variables, classes of thematic layers [27–30]. The FR is frequently used to map groundwater potential in a wide range of different circumstances [26,31–33]. In this model, the value of FR is computed from the thematic layers of the utilized factors that

identify groundwater availability [34]. This method uses a variety of criteria, derived from remote sensing data for the purpose of predicting groundwater occurrences. The study area was not undergoing extensive exploration using recent techniques of remote sensing and GIS. Therefore, the present study employs remote sensing data, field data, a GIS-based frequency ratio, and overlay analysis techniques to identify and combine data (twelve factors) derived from hydrologic, geological, climatic, and topographic factors in the Wadi Al Hamdh watershed area of Saudi Arabia in order to estimate the groundwater-promising zones, and to identify appropriate locations for artificial groundwater recharge.

## 2. Geologic and Hydrogeological Setting of the Study Area

The Wadi Al Hamdh basin includes Al-Madinah Governorate, while a few tributaries extend to Ha'il, Tabuk, and Makkah regions (Figure 1). Al-Madinah Al-Munawarah lies in the western part of the Arabian Peninsula that is considered a part of the Arabian Shield, comprising of Precambrian crystalline rocks, and underlying the alluvial sediments of the Quaternary age. Neoproterozoic basement rock units that comprise two groups of volcanic and sedimentary rocks [35] extend in the northern part of the Hijaz terrane [36] that comprises the Al Ays Group and Furayh Groups. The Saudi Arabian Paleozoic Sedimentary Strata (Paleozoic Sandstones) are known to crop out in a limited zone encompassing the Arabian Shield from the East and edge it to create the base of the Arabian Platform's enormous sedimentary strata from the West. The most significant and prolific "tight gas" and "shale gas" unconventional reservoirs are represented by it [37]. They have a thickness of roughly 500 m on the surface. Paleozoic sedimentary rocks are more than 4500 m thick in Saudi Arabia's subsoil [38].

Tertiary and Quaternary basalt are Neogene-Quaternary volcanics that make up the Cenozoic (Neogene-Quaternary) volcanics. The volcanic provinces of Neogene to Quaternary flood basalt known as the Harrat Rahat contain volcanic units. These Cenozoic basalts are unconformably deposited over both Precambrian rocks and wadi sediments close to Al-Madinah [39]. The uppermost weathered basalt flows are hydrologically connected units where groundwater is plentiful in the study region. Unconfined to semi-confined conditions are present in the groundwater. The Quaternary deposits (clay sand and gravel) in the Harrat Rahat were produced by the weathering of Precambrian rocks with exposures of basalt from the late Tertiary and Quaternary. The water table is between 28 and 93 m below the surface, while the sub-basaltic alluvial aquifer's groundwater level is from 535 to 594 m deep [40,41]. Instead of other sections in Al-Madinah, the direction of the water drain is from the west (Wadi Al Aqiq) towards the central and southern parts.

## 3. Data and Methods

To reveal potential prospective areas of groundwater in the Al-Madinah area, west of Saudi Arabia, a variety of satellite radar and optical data were gathered. To map the topographic features and determine the catchment characteristics, the SRTM DEM data were applied. Additionally, optical data were used to characterize the study area's land-use and cover (Figure 2). During the field study, groundwater data were collected, including the locations of groundwater wells, the density and distribution of irrigated farms, and flow discharge.

The USGS data resource center offers downloads of the SRTM DEM data with a spatial resolution of about 90 m. The watershed, stream networks, altitudes, slope, surface curvature, topographic wetness index (TWI), terrain roughness index (TRI), drainage density, and distance to river factors are used to define them using ArcGIS. The automatic delineation of stream extractions was carried out using the D8 approach [42]. For the purpose of determining other characteristics, the stream ordering was identified.

On 11 February 2013, Landsat 8 launched with the Landsat-OLI, an optical sensor with nine spectral bands. On 29 October 2022, two Level 1 scenes (path/row 170/043) of OLI data were obtained. The acquired images were masked and connected to the UTM Zone

37 N coordinate system. In this study, image enhancement and transformation methods were carried out using the OLI bands 2, 3, 4, 5, and 7.

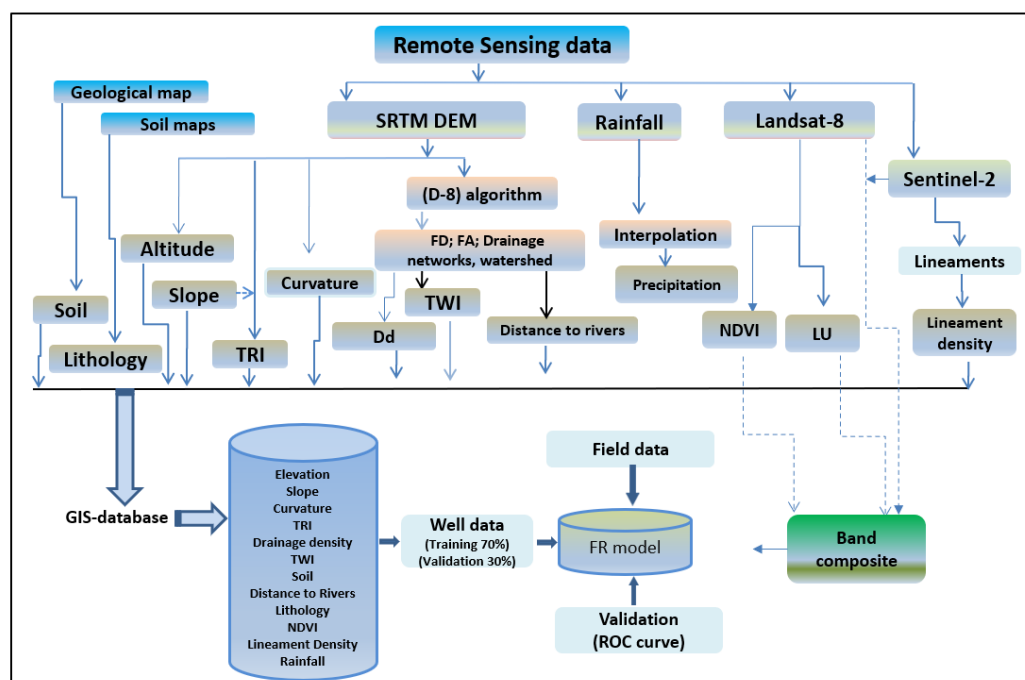


**Figure 2.** Diagram showing data and methods used in this study.

Multiple advanced very high-resolution radiometer (AVHRR) daily observations are computed to generate a nearly cloud-free image that exhibits the maximum amount of greenness. This is how the NDVI composites are created. A derived NDVI band composite is created by combining the NDVI ratio from bands one and two of the AVHRR composite. The data were downloaded from USGS EROS Archive-AVHRR NDVI Composites.

TRMM satellite recordings were used to obtain information on average rainfall. The obtained average rainfall statistics spanned from 1 January 1998 to 30 November 2015. They were spatially distributed using kriging interpolating tool. All such data are accessible at this URL: <https://giovanni.gsfc.nasa.gov/giovanni/> (accessed on 30 November 2016).

The Sentinel-2A satellite was launched on 23 June 2015, and the first data was collected a few days later. Sensors on Sentinel-2 collect information in the VIS/NIR, SWIR, and TIR wavelength ranges. The spatial resolution of these bands is 10–60 m. In total, 13 bands in the VIS/NIR and SWIR spectrum are recorded by Sentinel-2. The coastal band B1 (443 nm) has a 60 m pixel geometry, while the VIS/NIR bands have pixel sizes of 10 m for the blue B2 (490 nm), green B3 (560 nm), red B4 (665 nm), and infrared B8 (842 nm). The SWIR bands (B11: 1610 nm, B12: 2190 nm) have 20 m-wide pixels. Sentinel-2 scenario is provided in Sentinel’s proprietary SAFE format as zip-compressed files. JPEG files are used to preserve the spectral bands. In this SAFE file, the spectral bands are saved as jpg images with three distinct geometric resolutions (10 m, 20 m, and 60 m). A single GeoTIFF file with a uniform pixel size of 10 m is created by stacking the jpg files of bands B2, B3, B4, and B8 with a spatial resolution of 10 m and B11 and B12 with a resolution of 20 m. To minimize time and data calculation, a portion of these data were processed using SNAP software during preprocessing.

The classes of each thematic layer were done using the “Natural breaks classifier,” designed to optimally group similar values together and maximize the contrasts between classes (Jenks). A data clustering technique known as the Jenks optimization model, often known as the Jenks natural breaks classification method, aims to find the optimal grouping of values into several groups. Every thematic layer’s pixel was compared with the same spot in the applied overlay analysis. This means that several elements of the input eleven

layers should be combined to create a GWPZs map as the output. Noteworthy, each layer and subclass has a numerical rank assigned to it. This gives the user the ability to mathematically merge the layers and assign a new rank to each pixel in the final GWPZs map. The minimal input cell size (90 m) was integrated with the research area's GWPZs map, which represents the weighted average of the combined data-based maps (multi-criteria), in this model utilizing a weighted overlay method based on GIS. The below formula was used to do this.

$$\text{GWPZs} = \sum_{i=1}^n L_i \times F_i \quad (1)$$

where  $F_i$  refers to the strength of the inter-map (sub-class) features and  $L_i$  denotes the normalized weight of an evidentiary layer of the  $i$  parameter. This enables the eleven thematic maps to be blended according to the equation on a pixel basis.

## 4. Results

### 4.1. Elevation

Groundwater and surface runoff are influenced by altitude in terms of their direction and speed [43]. Elevation has a significant effect in revealing GWPZs [44]. As opposed to how it relates to the groundwater resource [45]. The areas of high altitude cannot hold precipitation that accumulates in areas of low topography in the downstream [14]. The study area's elevation map (Figure 3a) has been divided into five zones: 0–485, 485–756, 756–972, 972–1219, and 1219–2335 m, which cover, respectively, 7.81, 15.12, 38.89, 28.25, and 9.92% of the basin.



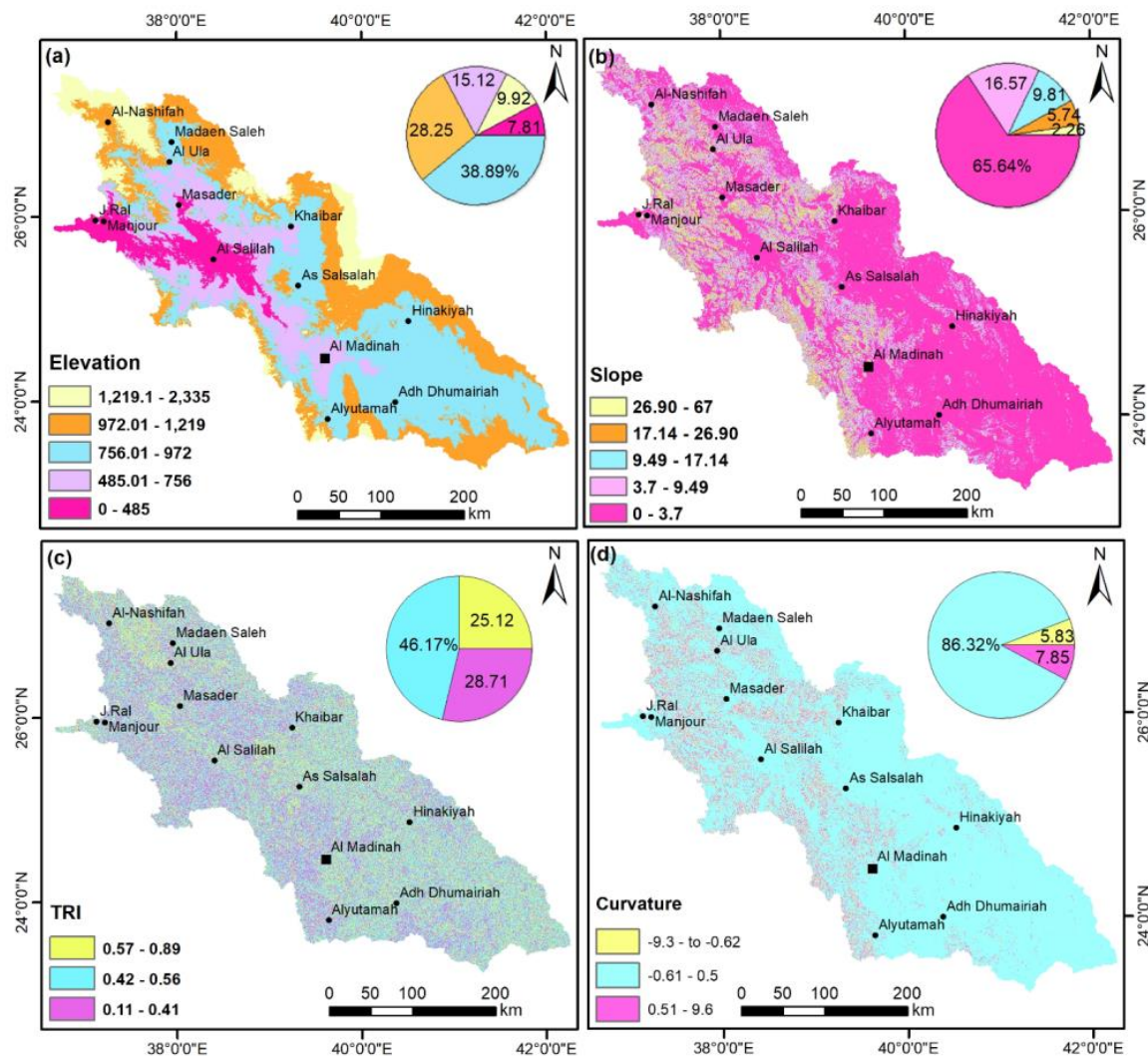


**Figure 3.** Topographic factors; (a) elevation; (b) slope; (c) TRI; (d) curvature.

#### 4.2. Slope

Slope is a prominent factor that controls groundwater potentiality and has a direct effect on the passage of rainwater [46]. Additionally, it can act as a broad guide to the direction of groundwater movement [47]. The amount of groundwater recharge is less at higher, steeper slopes because the water does not have enough time to percolate into the water table, and instead quickly spills over the surface. Conversely, the gentle slope plain areas can discharge the runoff water and increase the groundwater accumulation [48]. By affecting rates of surface infiltration and runoff as well as subsurface drainage, the slope angle regulates recharge [49]. The elevation map of the study area (Figure 3b) has been divided into five zones: 0–3.7, 3.7–9.49, 9.49–17.4, 17.14–26.90, and 26.90–67.25, which cover, respectively, 2.26, 5.74, 9.81, 16.57, and 65.64% of the basin.

#### 4.3. Terrain Roughness Index (TRI)

The terrain roughness index (TRI) is one of the geomorphic features that is related to the occurrence of groundwater potentiality. It was designed to evaluate landscape variability and can be used to explore for groundwater [50,51]. This variable can be determined using the following equation:

$$TRI = \sqrt{(max^2 - min^2)} \quad (2)$$

According to the buildup and infiltration of groundwater, the resulting TRI map was classified into five zones: 0.11 to 0.41 (low), 0.41 to 0.56 (moderate), and 0.56 to 0.89 (high) and 28.71, 46.17, and 25.12% of the basin are taken up by these regions.

#### 4.4. Curvature

The curvature of the land-surface is an important factor in water accumulation, percolation, and runoff [52,53]. It serves as a representation of the geometry of the land surface. The curvature layer, which is divided into three kinds: concave, convex, and flat, is produced using the DEM (Figure 3d). The land surface curvature can be used to locate areas that will capture rainwater runoff. Convex surfaces are less effective in collecting water than curved and flat areas, which also have a higher infiltration rate. An area with a high value of curvature is considered of high-grade value because water prefers to occur on flat and concave land surfaces [53]. The results were divided into three categories: low (−9.3 to −0.62), moderate (−0.61 to −0.5), and high (0.51–9.6).

#### 4.5. Drainage Density (Dd)

The Dd is one of the key indications of both the incidence and replenishment of groundwater [54]. It is the sum of all drainages in a basin divided by the sum of all its areas [55]. The Dd shows how the formation of the surface to the subsurface is distinct and it alludes inadvertently to the soil properties that determine soil infiltration ability [56]. Areas with low drainage density have higher levels of penetration and lower levels of runoff [16]. This implies that areas with lower drainage density are favorable for groundwater infiltration and productivity [57]. Therefore, the automatically extracted stream-networks (Figure 4a) in the study area are grouped into five classes: 0.028–0.14, 0.15–0.2, 0.21–0.24, 0.25–0.29, 0.30–0.39 that cover 9.47, 20.32, 27.19, 26.69, and 16.34, respectively (Figure 4b).

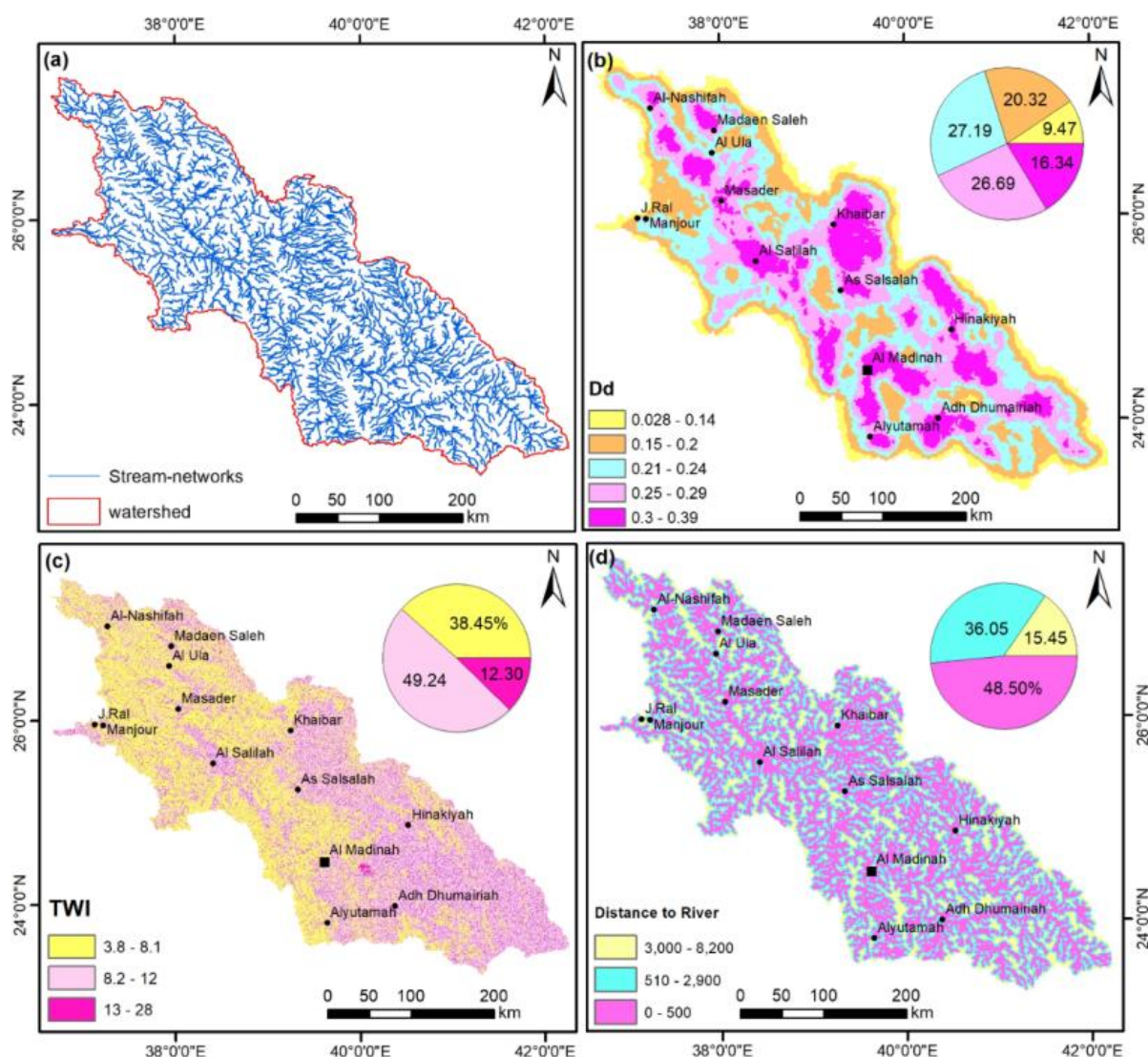


**Figure 4.** Hydrologic factors; (a) drainage-networks; (b) Dd; (c) TWI; (d) distance to river.

#### 4.6. Topographic Wetness Index (TWI)

The TWI is one of the crucial secondary terrain parameters that determine the availability of groundwater [58]. TWI identifies the connection-relationship between earth surface wetness and slope variation [59]. This index depicts how geography affects the amount of water that accumulates in an area. Therefore, steep slopes and higher elevations have more runoff, which reduces their ability for water storage. In contrast, low-lying areas have more ability for topographical wetness or water storage in the studied region [60]. The results of the TWI map were divided into three categories: low (3.8 to 8.1), moderate (8.1 to 12), and high (12 to 28), covering areas of 38.45, 49.24, and 12.30%, respectively (Figure 4c).

#### 4.7. Distance to River

Groundwater recharge in arid and mountainous terrain primarily results from infiltration from streams [61] during rainstorms. The separations between sites and streams are crucial signs indicating the possibility of groundwater extraction [62]. Groundwater recharge often declines the farther distance it is from streams. Therefore, the bedrock reservoirs in valleys contribute through stream leakage [58]. We used the Euclidean distance tool from the spatial analyst tools in Arc GIS 10 to extract the distance to river categories [21]. The resulted map (Figure 4d) is classified into three classes are 0–500, 500–2900, 2900–8200, which cover 15.45, 36.05, and 48.50, respectively.



#### 4.8. Lithology

Rock units have a direct correlation to recharge capability, where each type has a unique water body and rate of water recharge [63]. Porosity, permeability, and groundwater flow within the surface material are all impacted by the many forms of lithology and their properties, including texture and pore spaces [9,24,64]. Due to its recent deposition, higher permeability, and higher productivity, the Quaternary alluvial has good promise [65,66]. Therefore, the studied basin is classified into Precambrian, Cenozoic volcanics, Paleozoic sediments, and Quaternary deposits, which cover 61.63, 24.37, 9.83, and 4.17, respectively. It is noteworthy that Precambrian and Cenozoic volcanics cover most of the study area (Figure 5a).

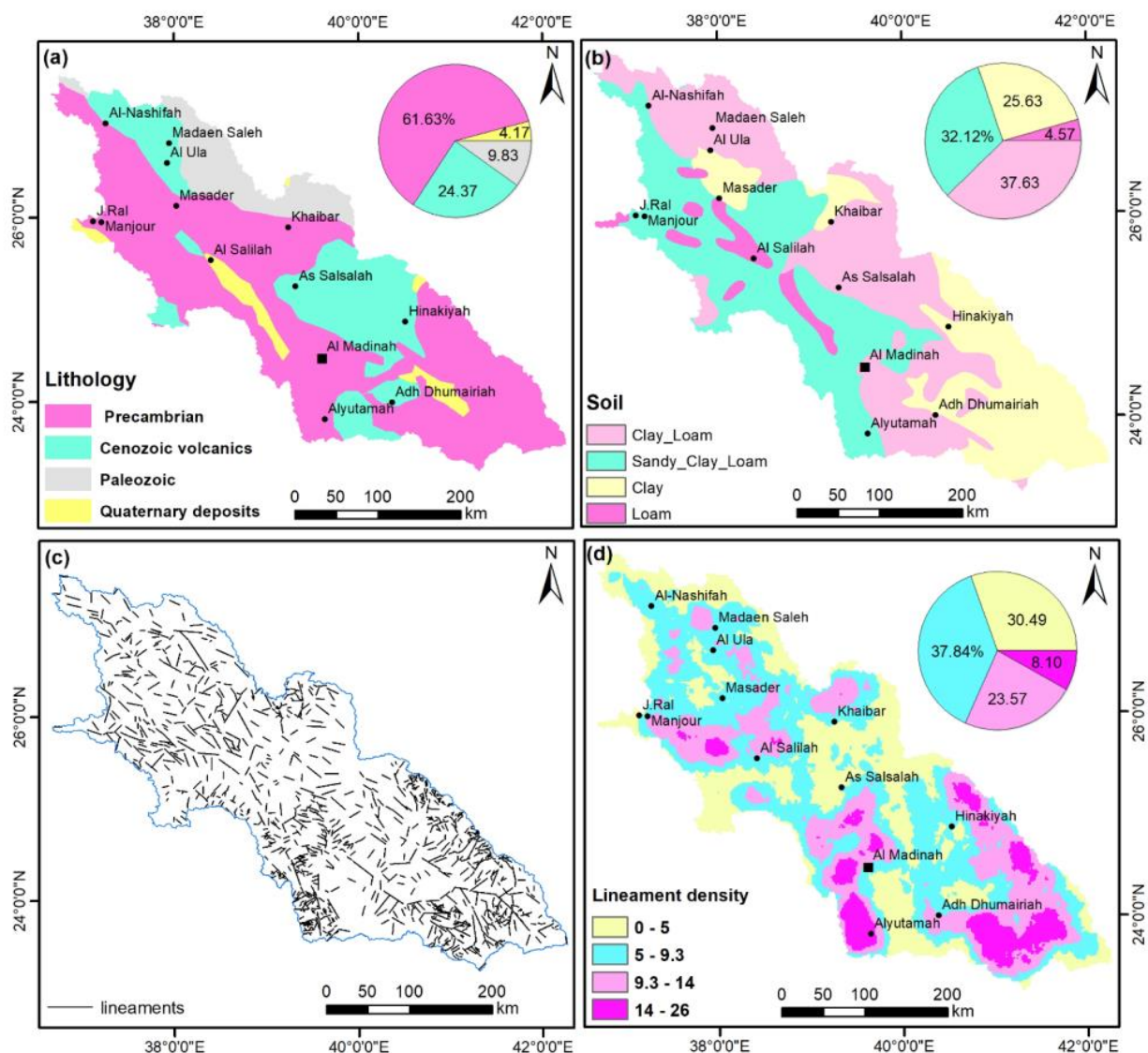


**Figure 5.** Geologic factors; (a) lithology; (b) soil; (c) lineaments; (d) lineament density map.

#### 4.9. Soil

Soil is a key geomorphological component of the porosity, permeability, and geometry of rocks. Hence, it represents an important factor in delineating the GPZs of a region. The amount of flow and infiltration is significantly influenced by the soil type [57]. Water movement can be significantly impacted by the size, shape, and arrangement of soil grains as well as their associated pore-systems [67]. Therefore, soil texture has a direct impact on porosity and permeability. Due to its permeability and porosity, fine-grained soil of a well sorted material such as sand has a lower rate of infiltration than coarse-grained

soil [68]. Considering that sandy soil has a high rate of penetration, coarser loamy soil with a high sand content has been given higher priority. In the meantime, fine soil with a lower infiltration rate due to a higher clay content has been given low priority [69]. The studied basin is occupied by clay loam, sandy clay loam, clay, and loam. These cover 37.63, 32.12, 25.63, and 4.57% of the area, respectively (Figure 5b).

#### 4.10. Lineaments

Deeper geological structures, such as faults, fractures, and ruptures with no discernible fracture displacement can be observed as lineaments on the surface of the earth's crust [70,71]. They serve as a conduit for the movement of groundwater, which results in an increase in secondary porosity and can therefore be used to identify potential groundwater zones [72]. Significant groundwater prospects could exist in a high-lineament density location. Lineaments offer crucial knowledge about surface and subsurface fracture systems, which may regulate the circulation and collection of groundwater [71,73,74]. This has been applied to identify possible locations for runoff water collection [75,76] and the distribution of groundwater resources. Higher lineament densities indicate permeability regions, which suggest promising regions for groundwater potential [71,77]. The lineaments (Figure 5c) of the studied basin were digitized from the Landsat and SRTM data, then they were converted to a lineament density map using Spatial Analyst of ArcGIS. The lineament density map is classified into four classes which are 0–5, 5–9.3, 9.3–14, 14–26, which cover 30.49, 37.84, 23.57, and 8.10%, respectively (Figure 5d).

#### 4.11. NDVI

The NDVI is a frequently used factor for groundwater potential zones [56,78]. The NDVI map was utilized to show the vegetation coverage and density. The NDVI layer was derived from data of the Advanced Very High-Resolution Radiometer (AVHRR). The NDVI ranges from  $-1$  to  $1$ , commonly referred to as 240 to 10,000; a higher NDVI value denotes dense vegetation. The NDVI result map of the study area ranges from 240 to 10,000 and is classified into four classes based on the natural break method which are 240–1000, 1000–1400, 1400–2600, and 2600–10,000, respectively (Figure 6a), and these cover areas of 37.36, 46.12, 15.90, and 0.62% of the area, respectively (Table 1).

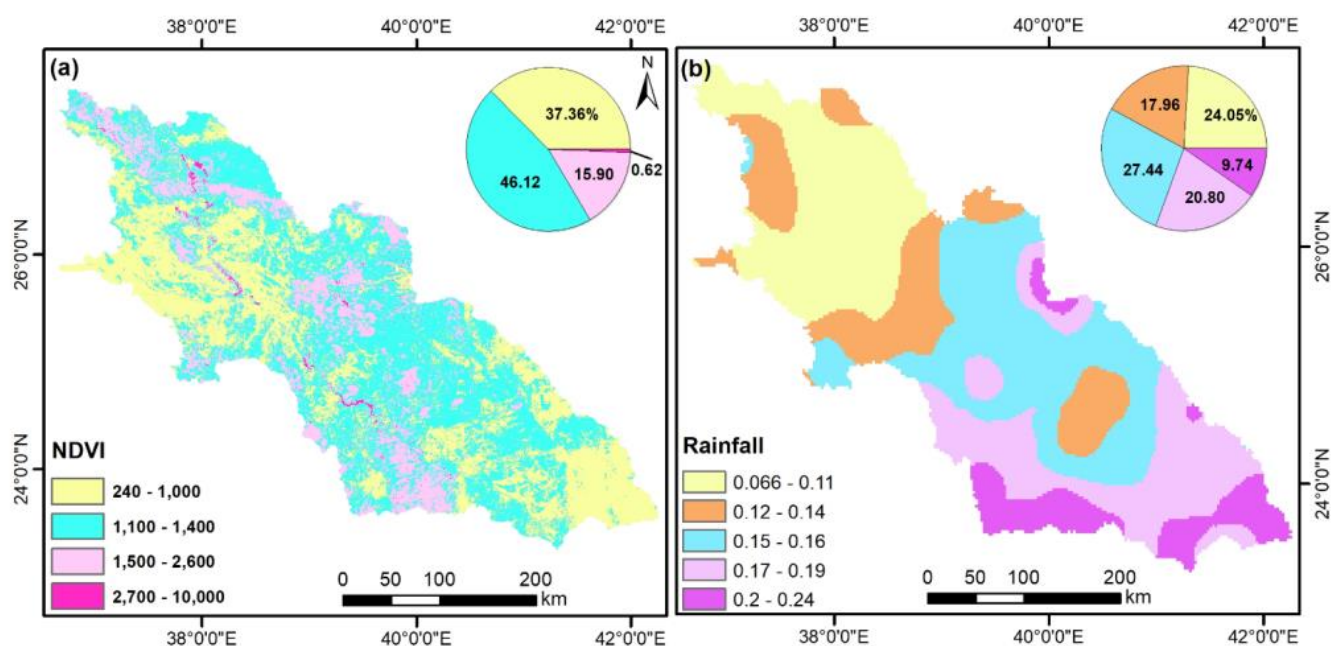


Figure 6. Ecologic and climatic factors; (a) NDVI distribution; (b) rainfall intensity.

**Table 1.** Factors influencing groundwater occurrence and computed FR values.

Topography	No .Pixels in Domain	Domain %	No. Wells	No. Wells %	FR
0–485	1,046,241	0.078	36	0.12	1.47
485.01–756	2,025,026	0.151	156	0.50	3.30
756.01–972	5,207,302	0.389	116	0.37	0.95
972.01–1219	3,782,988	0.283	4	0.01	0.05
1219.1–2335	1,328,281	0.099	1	0.00	0.03
Slope classes					
0–3.7	8,768,661	0.656	266	0.85	1.29
3.7–9.49	2,213,055	0.166	33	0.11	0.64
9.49–17.14	1,310,133	0.098	8	0.03	0.26
17.14–26.90	766,364	0.057	4	0.01	0.22
26.90–67.25	301,435	0.023	2	0.01	0.28
Dd					
0.028–0.14	2416	0.095	2	0.01	0.07
0.15–0.2	5185	0.203	21	0.07	0.33
0.21–0.24	6939	0.272	55	0.18	0.65
0.25–0.29	6813	0.267	113	0.36	1.35
0.3–0.39	4170	0.163	122	0.39	2.39
NDVI					
235–1043	268,046	0.374	32	0.10	0.27
1043–1380	330,950	0.461	72	0.23	0.50
1380–2639	114,115	0.159	127	0.41	2.55
2639–10,000	4419	0.006	82	0.26	42.54
Dist to Rivers					
0–500	12,371	0.485	258	0.82	1.70
510–2900	9194	0.360	47	0.15	0.42
3000–8200	3940	0.154	8	0.03	0.17
TRI					
0.11–0.41	3,852,555	0.287	103	0.33	1.15
0.42–0.56	6,194,486	0.462	120	0.38	0.83
0.57–0.89	3,370,565	0.251	90	0.29	1.14
Lineament density					
0–5	9813	0.305	6	0.20	0.66
5–9.3	12,178	0.378	4	0.13	0.35
9.3–14	7587	0.236	7	0.23	0.99
15–26	2608	0.081	13	0.43	5.35
Soil					
Clay_Loam	7,226,776	0.377	142	0.45	1.20
Sandy_Clay_Loam	6,161,094	0.321	84	0.27	0.84
Clay	4,914,699	0.256	38	0.12	0.47
Loam	876,276	0.046	49	0.16	3.43

Table 1. Cont.

Topography	No .Pixels in Domain	Domain %	No. Wells	No. Wells %	FR
Rainfall					
0.066–0.11	3925	0.241	101	0.32	1.34
0.12–0.14	2931	0.180	11	0.04	0.20
0.15–0.16	4477	0.274	90	0.29	1.05
0.17–0.19	3394	0.208	95	0.30	1.46
0.2–0.24	1590	0.097	16	0.05	0.52
Curvature					
neg 9.3 to neg 0.64	781,089	0.058	9	0.03	0.49
neg 0.62 to 0.5	11,557,636	0.863	298	0.95	1.10
0.51–9.6	1,051,113	0.079	6	0.02	0.24
TWI					
3.8–8.1	5,137,005	0.385	64	0.20	0.53
8.2–12	6,578,827	0.492	185	0.59	1.20
13–28	1,643,816	0.123	64	0.20	1.66
GEOLOGY					
Precambrian	19,975	0.616	218	0.70	1.13
Cenozoic volcanics	7897	0.244	79	0.25	1.04
Paleozoic	3187	0.098	5	0.02	0.16
Quaternary deposits	1351	0.042	11	0.04	0.84

#### 4.12. Rainfall Data (TRMM)

Water availability in a network is defined by rainfall patterns. Thus, the amount of rainfall is one of the crucial factors in identifying groundwater potential zones and is the hydrologic method of recharging aquifers [54]. Rainfall causes a particular land area's likelihood of having groundwater to rise [79]. Using rainfall information from the TRMM data, researchers may monitor, record, and measure the downpour rates within the examined watershed. The main sources of groundwater are infiltration and drainage from precipitation. It is the primary natural recharge source that initiates groundwater supplies [19,80]. The rainfall intensity map was classified into five classes which are 0.066–0.11, 0.11–0.14, 0.15–0.16, 0.16–0.19, and 0.20–0.24, which cover 24.05, 17.96, 27.44, 20.80, and 9.74, respectively (Figure 6b). Rainfall allows accumulation that facilitates groundwater infiltration, which replenishes the shallow acquirers (Figure 7), as the area was recently hit by rainfall storms.





**Figure 7.** Rainfall accumulation during the storm on 3 January 2023.

### 5. Groundwater Potential Mapping

Utilizing the FR model, we determined the locations of the wells (nearness for the groundwater) and the controlling factors (Table 1). FR values below 1 are thought to suggest weak correlations, while those above 1 are thought to show strong correlations [26,81]. The highest FRs were found in the elevation classes from 485–756 (3.30), followed by those from 0 to 485 (1.47), but the lowest FR was found in the elevation classes from 1219 to 2335 (0.03). This was the case for areas with lower elevation which are more likely to hold groundwater than higher elevation [16]. This correlated with areas of low slope that positively related to high groundwater potential. The areas with slopes from 0 to 3.7 had high FRs (1.29) but steep slopes 26.9–67.25 (0.28). Noteworthy, areas with lower TRIs (from 0.11 to 0.41) have the highest FR's values (1.15) that are followed by 0.57–0.89 (1.14) but the class of 0.42–0.56 (0.83) is the lowest (Table 1). Additionally, the curvature class  $-0.62$  to  $0.5$  is the highest value, 1.103, that almost reveals areas that are almost flat, but areas of highest curvature displayed a low FR value (0.244).

The Dd classes display a positive correlation and steady increase with the FR values (Table 1). The zones with high Dd values (from 0.3 to 0.39) have greater FRs (2.38), whereas the regions with low Dd values have the lowest FRs (Table 1). Likewise, the TWI classes with higher values reveal higher FR values e.g., from 3.87 to 8.1 (FR = 0.53), followed by the TWI classes from 8.2 to 12 (FR = 1.20) and from 13 to 28 (FR = 1.66). Additionally, the values of the FR show a negative association as river distance increases. From 0 to 500, the locations closest to the rivers had the highest FRs (1.7), whilst the locations further away from the rivers had poor potentiality (FR = 0.165).

In terms of geologic characteristics, the Precambrian rocks display a high FR value (1.13) that is followed by Cenozoic volcanics (1.04), and Quaternary deposits (0.84), but the Paleozoic rock unit has the lowest (0.16). Loam, and clay loam classes have the highest, 3.43 and 1.20, respectively, but clay soil is the lowest (0.47). Furthermore, the higher the lineament density values, the higher the FR values, e.g., 0 to 5 (FR = 0.656; lowest) but 15–26 (FR = 5.34; the highest). The NDVI class displays a strong positive correlation with FR values. The NDVI classes with higher values, 2639–10,000, have FR = 42.54, but with low NDVIs from 235 to 1043 have the lowest (FR = 0.27). In terms of the rainfall classes, the areas that received from 0.17 to 0.19 mm/day had the highest FR value (1.46), followed by those that received from 0.066 to 0.11 mm (FR = 1.34).

The twelve evidential layers are combined based on the discussed FR values. Following that, we divided the combined groundwater potential zones (GWPZs) map, created by combining 12 thematic maps, with the natural breaks method into five categories (Figure 8a: 2.24, 5.81, 13.39, 53.90, and 24.65%). These, respectively, are very good, good, moderate,

low, and very low. Using the ROC curve, the GWPZ map of the study area is validated (Figure 9). The AUC can be used to describe the system's capacity to accurately predict both the occurrence of "groundwater" and its absence, which emphasizes the value of its estimate. AUC values vary from 0 to 1, with smaller values suggesting a more useful prediction, and greater values reflecting more accurate estimates. The AUC result of the model is 0.893, representing better accuracy. The field observations validated the GWPZ map as several wells are consistent with the zones of high potentiality. Additionally, several farms coincide with those zones (Figure 10). Vegetation and water resources make up the majority of the extremely high to extreme GWPZs, according to the Landsat-9 band composites 7, 5, and 3 (Figure 11a–c) and Sentinel-2 (Figure 11d,e).

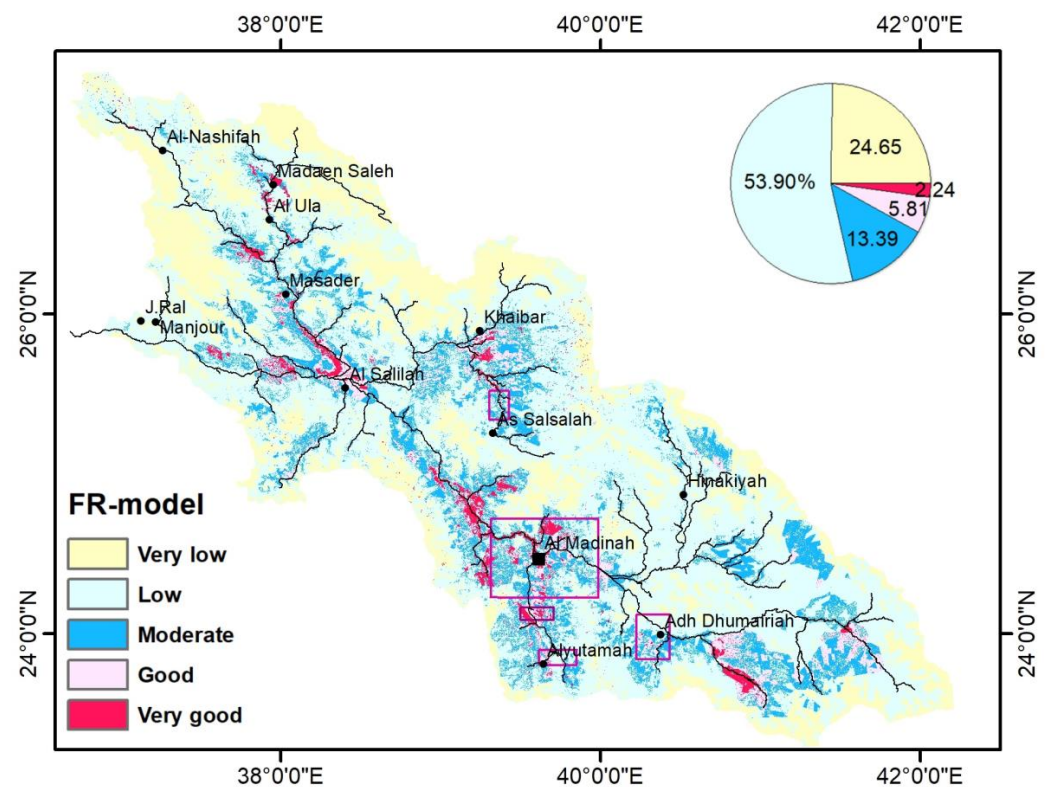


Figure 8. Groundwater potential zone map using FR-model and validated field data.

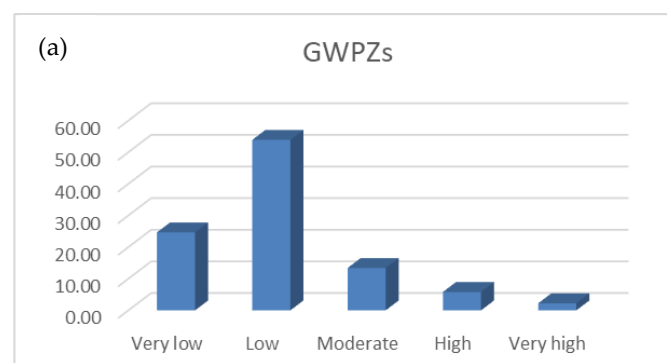
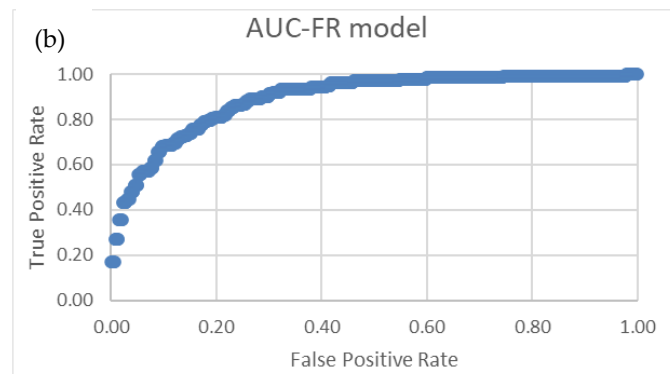


Figure 9. Cont.



**Figure 9.** (a) GWPZ areas of predicted model; (b) AUCs of predicted GWPZ.



**Figure 10.** Field observations (a) Madaen Saleh; (b) Al Ula area displays the pumping well and vegetated area; (c–e) water wells at Al Madinah; (f) Al Yutamah area that is enriched in date palm trees; (g) Wadi Aqiq surface water flow during rainy storms.



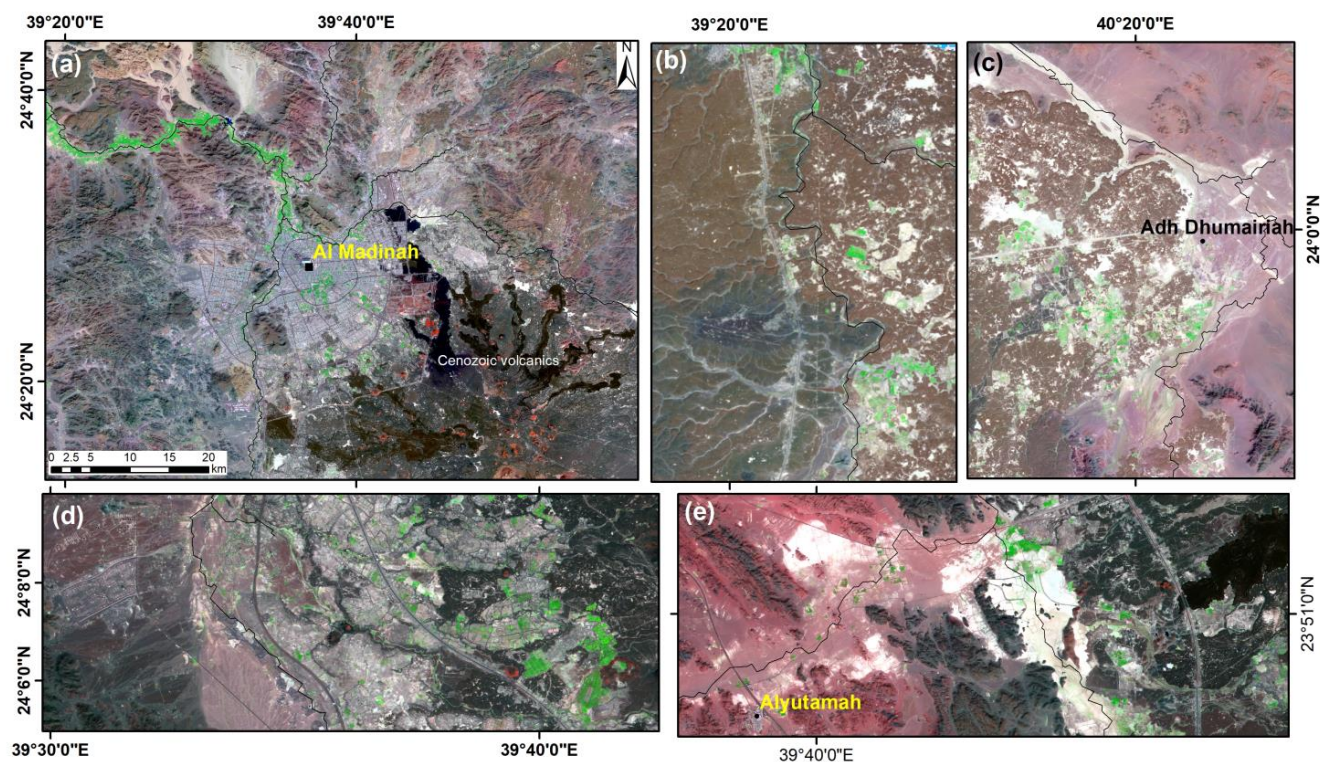


**Figure 11.** Landsat-9 of the study area (a) vegetated areas around Al Madinah and Quaternary volcanics in black; (b) Al Yutamah farms south of Al Madinah; (c) Adh Dhumainah farms south of Al Madinah; (d) band combination 12, 8, 3 of Sentinel-2 of the area south of Al Madinah; (e) Sentinel-2 of Alyutamah area reveal the signature of surface water in a bright tone. Polygon in magenta color in Figure 8 is the reference location for these sub-figures.

## 6. Discussion

Using the FR model, we determine here the spatial relations between features and controlling factors (Table 1). Areas of low elevation and slope are more likely to hold groundwater than higher elevation [14,16,79]. This correlated with areas of low slope that are positively related to high groundwater potential. In terms of the hydrologic properties, the Dd reveals areas of high FR values and groundwater potentiality. The groundwater potential was promising for the highest TWI classes as TWI positively correlated with FR values [26]. The areas close to the streams from 0 to 500 had the highest FRs (1.7) which reveals that the nearness to the streams results in more recharging capability. However, areas farther from the rivers had low potentiality. In terms of geologic properties, the Precambrian rocks display a high FR value and groundwater potential, as such areas are dominated by basement rocks that hold groundwater in a fractured aquifer. This coincides with the FR values that are higher with the lineament density as the Precambrian and Cenozoic volcanic rocks must have fractures to hold groundwater. The groundwater potential probability has a strong positive correlation with NDVI values, as the highest FR values coincide with the occurrence of vegetation and hence groundwater in arid regions [26] and rainfall intensity. Although the area is characterized by rugged terrain with limited rainfall, combining the evidential layers revealed that good and very good zones cover ~8% of the study region.

Basement rocks and brecciated vesicular basalts in the area are overlain by alluvium that is composed of breccia and conglomerates, and the siltstone and the claystone (Figure 12). Such rock units that are highly fracture, represent the main aquifer system that is recharged by the structurally controlled drainage pattern, e.g., parallel drainage in a northwesterly direction probably related to the Najd Fault System along with the N-S and the cross-cutting E-W Cenozoic trans tensional faults. The latter are related to the Red



Sea Opening [82]. Water occurrences can be significantly controlled by the size, shape, and arrangement of soil grains, as well as their associated pores systems. Therefore, fine-grained soil of well sorted material such as sand has a lower rate of infiltration than coarse-grained soil [68]. Accordingly, loam, sandy clay loam, and clay loam classes which occupy about 75% of the area have the highest FR values but clay soil has the lowest.



**Figure 12.** Vegetated areas at Wadi Al Ula Town. These are irrigated using groundwater wells abstracted from clastic Paleozoic rocks aquifer. Wadi Al Qura passes through Al Ula town, formed by Tertiary N-S graben system that deformed the Paleozoic rocks.

The Wadi Al-Aqiq valley connects all valleys at Al-Ayoun in Al-Madinah Al-Munawarah, providing a 150 km recharging region south of Al-Madinah. It discharges its water in a trellised drainage pattern. The Wadi Qanah-Al-Hamdh watershed connects all the valleys in the Al-Madinah and flows from the southeast to the northwest. It is >400 km long and around 150 km wide [83]. The three mentioned sub-basins flow in the Tayef region; the Wadi Qanah-Al-Aqul valley is 300 kilometres southeast of Al-Madinah. These valleys' watersheds display a trellised structure of drainage, which may be related to the Red Sea Rift. Additionally, groundwater wells that draw water from an aquifer of clastic Paleozoic rock are used to irrigate vegetation in Al Ula Town (Figure 12).

## 7. Conclusions

In arid and hyper-arid locations, groundwater is especially a crucial supply of water for sustainable development. To reveal, evaluate, and monitor exploration data for water resources in various climatic situations, RS data and GIS-techniques are effectively merged. W. Al-Hamdh, in the Al-Madinah Al-Munawarah area, in the western part of Saudi Arabia was investigated using remote sensing and GIS techniques. The main goal was to identify prospective zones of groundwater potential and recharge zones. Here, we integrated twelve GIS thematic layers that depict the geology, geomorphic, climatic, and hydrologic conditions. These layers are soil, lithology, slope, elevation, curvature, TRI, Dd, TWI, distance to river, rainfall, NDVI, and lineament density. They were processed, normalized and integrated using GIS-based FR-overlay model. The result revealed the groundwater prospective areas, which are here categorized into five zones: very good, good, moderate, low, and very low that covering 2.24, 5.81, 13.39, 53.90, and 24.65% of the entire area. Field observation and the AUC validated the model which presented good performance (AUC: 0.893). The promising areas represent the artificial abstraction for groundwater supply. Overall, decision-makers and sustainability considerations greatly benefit from resultant GWPZ using RS and GIS. Moreover, this approach can be applied on a regional scale and in areas with comparable conditions.

**Author Contributions:** Conceptualization, M.A. and F.A.; methodology, M.A.; software, M.A.; validation, F.A., A.O.B. and N.A.-A.; investigation, M.A.; resources, N.A.-A.; writing—original draft preparation, M.A., F.E.-B. and A.O.B.; writing—review and editing, M.A. and F.E.-B. All authors have read and agreed to the published version of the manuscript.

**Funding:** This research received no external funding.

**Data Availability Statement:** Not applicable.

**Acknowledgments:** Nasir Al-Arifi extends his grateful to the Deanship of Scientific Research, King Saud University for funding through the Vice Deanship of Scientific Research Chairs.

**Conflicts of Interest:** The authors declare no conflict of interest.

## References

1. The United Nations World Water Development Report 2018 (WWDR). In *Nature-Based Solutions for Water*; UNESCO: Paris, France, 2018.
2. World Health Organization (WHO). *Progress on Sanitation and Drinking Water: 2015 Update and MDG Assessment*; WHO: Geneva, Switzerland, 2015.
3. Chow, V.T.; Maidment, D.R.; Mays, L.W. *Applied Hydrology*; McGraw-Hill Book Co.: Singapore, 1988.
4. Black, M.; Talbot, R. *Water, a Matter of Life and Health: Water Supply and Sanitation in Village India*; Oxford University Press: Noida, India, 2005.
5. Holden, J. *Water Resources: An Integrated Approach*; Routledge: New York, NY, USA, 2014.
6. Molden, D. Water responses to urbanization. *Paddy Water Environ.* **2007**, *5*, 207–209. [[CrossRef](#)]
7. Abd Manap, M.; Nampak, H.; Pradhan, B.; Lee, S.; Sulaiman, W.N.A.; Ramli, M.F. Application of probabilistic-based frequency ratio model in groundwater potential mapping using remote sensing data and GIS. *Arab. J. Geosci.* **2014**, *7*, 711–724. [[CrossRef](#)]
8. Arulbalaji, P.; Padmalal, D.; Sreelash, K. GIS and AHP techniques based delineation of groundwater potential zones: A case study from Southern Western Ghats. *India Sci. Rep.* **2019**, *9*, 2082. [[CrossRef](#)] [[PubMed](#)]
9. Abdelkareem, M.; Al-Arifi, N. The use of remotely sensed data to reveal geologic, structural, and hydrologic features and predict potential areas of water resources in arid regions. *Arab. J. Geosci.* **2021**, *14*, 704. [[CrossRef](#)]
10. Barlow, M.; Clarke, T. *Blue Gold: The Fight to Stop the Corporate Theft of the World's Water*; The New Press: New York, NY, USA, 2002.
11. Hutti, B.; Nijagunappa, R. Identification of groundwater potential zone using Geoinformatics in Ghataprabha basin, North Karnataka, India. *Int. J. Geomat. Geosci.* **2011**, *2*, 91–109.
12. Naghibi, S.A.; Vafakhah, M.; Hashemi, H.; Pradhan, B.; Alavi, S.J. Groundwater augmentation through the site selection of floodwater spreading using a data mining approach (case study: Mashhad Plain, Iran). *Water* **2018**, *10*, 1405. [[CrossRef](#)]
13. Chen, W.; Zhao, X.; Tsangaratos, P.; Shahabi, H.; Ilia, I.; Xue, W.; Wang, X.; Ahmad, B.B. Evaluating the usage of tree-based ensemble methods in groundwater spring potential mapping. *J. Hydrol.* **2020**, *583*, 124602. [[CrossRef](#)]
14. Abdelkareem, M.; Abdalla, F. Revealing potential areas of water resources using integrated remote-sensing data and GIS-based analytical hierarchy process. *Geocarto Int.* **2021**, *37*, 8672–8696. [[CrossRef](#)]
15. Jha, M.K.; Chowdhury, A.; Chowdary, V.M.; Peiffer, S. Groundwater management and development by integrated remote sensing and geographic information systems: Prospects and constraints. *Water Resour. Manag.* **2007**, *21*, 427–467. [[CrossRef](#)]
16. Sun, T.; Cheng, W.; Abdelkareem, M.; Al-Arifi, N. Mapping Prospective Areas of Water Resources and Monitoring Land Use/Land Cover Changes in an Arid Region Using Remote Sensing and GIS Techniques. *Water* **2022**, *14*, 2435. [[CrossRef](#)]
17. Salman, S.A.; Shahid, S.; Mohsenipour, M.; Asgari, H. Impact of land use on groundwater quality of Bangladesh. *Sustain. Water Resour. Manag.* **2018**, *4*, 1031–1036. [[CrossRef](#)]
18. Elmahdy, S.I.; Mohamed, M.M. Probabilistic frequency ratio model for groundwater potential mapping in Al Jaww plain, UAE. *Arab. J. Geosci.* **2015**, *8*, 2405–2416. [[CrossRef](#)]
19. Avand, M.; Janizadeh, S.; Tien Bui, D.; Pham, V.H.; Ngo, P.T.T.; Nhu, V.-H. A tree-based intelligence ensemble approach for spatial prediction of potential groundwater. *Int. J. Digit. Earth* **2020**, *13*, 1408–1422. [[CrossRef](#)]
20. Nguyen, P.T.; Ha, D.H.; Jaafari, A.; Nguyen, H.D.; Van Phong, T.; Al-Ansari, N.; Prakash, I.; Le, H.V.; Pham, B.T. Groundwater Potential Mapping Combining Artificial Neural Network and Real AdaBoost Ensemble Technique: The DakNong Province Case-study, Vietnam. *IJERPH* **2020**, *17*, 2473. [[CrossRef](#)]
21. Jaafarzadeh, M.S.; Tahmasebipour, N.; Haghizadeh, A.; Pourghasemi, H.R.; Rouhani, H. Groundwater recharge potential zonation using an ensemble of machine learning and bivariate statistical models. *Sci. Rep.* **2021**, *11*, 5587. [[CrossRef](#)]
22. Davoodi, M.D.; Rezaei, M.; Pourghasemi, H.R.; Pourtaghi, Z.S.; Pradhan, B. Groundwater spring potential mapping using bivariate statistical model and GIS in the Taleghan watershed Iran. *Arab. J. Geosci.* **2013**, *8*, 913–929. [[CrossRef](#)]
23. Pourtaghi, Z.S.; Pourghasemi, H.R. GIS-based groundwater spring potential assessment and mapping in the Birjand Township, southern Khorasan Province, Iran. *Hydrogeology* **2014**, *22*, 643–662. [[CrossRef](#)]

24. Naghibi, S.A.; Pourghasemi, H.R. A comparative assessment between three machine learning models and their performance comparison by bivariate and multivariate statistical methods in groundwater potential mapping. *Water Resour. Manag.* **2015**, *29*, 5217–5236. [\[CrossRef\]](#)
25. Maity, B.; Mallick, S.K.; Das, S.; Rudra, S. Comparative analysis of groundwater potentiality zone using fuzzy AHP, frequency ratio and Bayesian weights of evidence methods. *Appl. Water Sci.* **2022**, *12*, 12–63. [\[CrossRef\]](#)
26. Li, Y.; Abdelkareem, M.; Al-Arifi, N. Mapping Potential Water Resource Areas Using GIS-Based Frequency Ratio and Evidential Belief Function. *Water* **2023**, *15*, 480. [\[CrossRef\]](#)
27. Oh, H.J.; Kim, Y.S.; Choi, J.K.; Park, E.; Lee, S. GIS mapping of regional probabilistic groundwater potential in the area of Pohang City, Korea. *J. Hydrol.* **2011**, *399*, 158–172. [\[CrossRef\]](#)
28. Razandi, Y.; Pourghasemi, H.R.; Neisani, N.S.; Rahmati, O. Application of analytical hierarchy process, frequency ratio, and certainty factor models for groundwater potential mapping using GIS. *Earth Sci. Inform.* **2015**, *8*, 867–883. [\[CrossRef\]](#)
29. Arshad, A.; Zhang, Z.; Zhang, W.; Dilawar, A. Mapping favorable groundwater potential recharge zones using a GIS-based analytical hierarchical process and probability frequency ratio model: A case study from an agro-urban region of Pakistan. *Geosci. Front.* **2020**, *11*, 1805–1819. [\[CrossRef\]](#)
30. Yariyan, P.; Avand, M.; Omidvar, E.; Pham, Q.B.; Linh, N.T.T.; Tiefenbacher, J.P. Optimization of statistical and machine learning hybrid models for groundwater potential mapping. *Geocarto Int.* **2020**, *11*, 2282–2314. [\[CrossRef\]](#)
31. Das, S. Comparison among influencing factor, frequency ratio, and analytical hierarchy process techniques for groundwater potential zonation in Vaitarna basin, Maharashtra, India. *Groundw. Sustain. Dev.* **2019**, *8*, 617–629. [\[CrossRef\]](#)
32. Siahkamari, S.; Haghizadeh, A.; Zeinivand, H.; Tahmasebipour, N.; Rahmati, O. Spatial prediction of food-susceptible areas using frequency ratio and maximum entropy models. *Geocarto Int.* **2018**, *33*, 927–941. [\[CrossRef\]](#)
33. Razavi-Termeh, S.V.; Sadeghi-Niaraki, A.; Choi, S.-M. Groundwater potential mapping using an integrated ensemble of three bivariate statistical models with random forest and logistic model tree models. *Water* **2019**, *11*, 1596. [\[CrossRef\]](#)
34. Balamurugan, G.; Seshan, K.; Bera, S. Frequency ratio model for groundwater potential mapping and its sustainable management in cold desert India. *J. King Saud Univ.-Sci.* **2017**, *29*, 333–347.
35. Pellaton, C. *Geologic Map of the Al Madinah Quadrangle, Sheet 24D, Kingdom of Saudi Arabia: Saudi Arabian Deputy Ministry for Mineral Resources Geosciences Map GM-52, Scale 1:250,000*; Pascal and Francis: Orono, ME, USA, 1981; p. 19.
36. Johnson, P.R. *Explanatory Notes to the Map of Proterozoic Geology of Western Saudi Arabia: Saudi Geological Survey Technical Report SGS-TR-2006-4*; Saudi Geological Survey: Jeddah, Kingdom of Saudi Arabia, 2006; p. 62, 22 figs., 2 plates.
37. Yassin, M.A.; Abdullatif, O.M. Chemostratigraphic and sedimentologic evolution of Wajid group (Wajid sandstone): An outcrop analog study from the cambrian to permian, SW Saudi Arabia. *J. Afr. Earth Sci.* **2017**, *126*, 159–175. [\[CrossRef\]](#)
38. Al-Ajmi, H.F.; Keller, M.; Hinderer, M.; Filomena, C.M. Lithofacies, depositional environments and stratigraphic architecture of the Wajid Group outcrops in southern Saudi Arabia. *GeoArabia* **2015**, *20*, 49–94. [\[CrossRef\]](#)
39. Coleman, R.G.; Gregory, R.T.; Brown, G.F. *Cenozoic Volcanic Rocks of Saudi Arabia: Saudi Arabian Deputy Ministry for Mineral Resources Open-File Report USGS-OF-03-93*; U.S. Geological Survey: Reston, VA, USA, 1983; p. 82.
40. Bamousa, A.O.; El Maghraby, M. Groundwater characterization and quality assessment, and sources of pollution in Madinah, Saudi Arabia. *Arab. J. Geosci.* **2016**, *9*, 536. [\[CrossRef\]](#)
41. Metwaly, M.; Abdalla, F.; Taha, A. Hydrogeophysical Study of Sub-Basaltic Alluvia Aquifer in the Southern Part of Al-Madinah Al-Munawarah, Saudi Arabia. *Sustainability* **2021**, *13*, 9841. [\[CrossRef\]](#)
42. O'Callaghan, J.F.; Mark, D.M. The extraction of drainage networks from digital elevation data. *Comput. Vis. Graph. Image Process.* **1984**, *28*, 323–344. [\[CrossRef\]](#)
43. Yousefi, S.; Sadhasivam, N.; Pourghasemi, H.R.; Ghaffari Nazarlou, H.; Golkar, F.; Tavangar, S.; Santosh, M. Groundwater spring potential assessment using new ensemble data mining techniques. *Measurement* **2020**, *157*, 107652. [\[CrossRef\]](#)
44. Naghibi, S.A.; Pourghasemi, H.R.; Dixon, B. GIS-based groundwater potential mapping using boosted regression tree, classification and regression tree, and random forest machine learning models in Iran. *Environ. Monit. Assess.* **2016**, *188*, 44. [\[CrossRef\]](#)
45. Karimi-Rizvandi, S.; Goodarzi, H.V.; Afkoeieh, J.H.; Chung, I.-M.; Kisi, O.; Kim, S.; Linh, N.T.T. Groundwater-potential mapping using a self-learning bayesian network model: A comparison among metaheuristic algorithms. *Water* **2021**, *13*, 658. [\[CrossRef\]](#)
46. Al Saud, M. Mapping potential areas for groundwater storage in Wadi Aurnah Basin, western Arabian Peninsula, using remote sensing and geographic information system techniques. *Hydrogeol. J.* **2018**, *18*, 1481–1495. [\[CrossRef\]](#)
47. Gupta, M.; Srivastava, P.K. Integrating GIS and remote sensing for identification of groundwater potential zones in the hilly terrain of Pavagarh, Gujarat, India. *Water Int.* **2010**, *35*, 233–245. [\[CrossRef\]](#)
48. Kaewdum, N.; Chotpantarat, S. Mapping Potential Zones for Groundwater Recharge Using a GIS Technique in the Lower Khwae Hanuman Sub-Basin Area, Prachin Buri Province, Thailand. *Front. Earth Sci.* **2021**, *9*, 717313. [\[CrossRef\]](#)
49. Naghibi, S.A.; Dolatkordestani, M.; Rezaei, A.; Amouzegari, P.; Heravi, M.T.; Kalantar, B.; Pradhan, B. Application of rotation forest with decision trees as base classifier and a novel ensemble model in spatial modeling of groundwater potential. *Environ. Monit. Assess.* **2019**, *191*, 248. [\[CrossRef\]](#)
50. Kalantar, B.; Al-Najjar, H.A.H.; Pradhan, B.; Saeidi, V.; Halin, A.A.; Ueda, N.; Naghibi, S.A. Optimized Conditioning Factors Using Machine Learning Techniques for Groundwater Potential Mapping. *Water* **2019**, *11*, 1909. [\[CrossRef\]](#)



51. Moghaddam, D.D.; Rahmati, O.; Haghizadeh, A.; Kalantari, Z. A Modeling Comparison of Groundwater Potential Mapping in a Mountain Bedrock Aquifer: QUEST, GARP, and RF Models. *Water* **2020**, *12*, 679. [\[CrossRef\]](#)
52. Benjmel, K.; Amraoui, F.; Boutaleb, S.; Ouchchen, M.; Tahiri, A.; Touab, A. Mapping of Groundwater Potential Zones in Crystalline Terrain Using Remote Sensing, GIS Techniques, and Multicriteria Data Analysis (Case of the Ighrem Region, Western Anti-Atlas, Morocco). *Water* **2020**, *12*, 471. [\[CrossRef\]](#)
53. Mukherjee, I.; Singh, U.K. Delineation of groundwater potential zones in a drought-prone semi-arid region of east India using GIS and analytical hierarchical process techniques. *CATENA* **2020**, *194*, 104681. [\[CrossRef\]](#)
54. Magesh, N.S.; Chandrasekar, N.; Soundranayagam, J.P. Delineation of groundwater potential zones in Theni district, Tamil Nadu, using remote sensing, GIS and MIF techniques. *Geosci. Front.* **2012**, *3*, 189–196. [\[CrossRef\]](#)
55. Tolche, A.D. Groundwater potential mapping using geospatial techniques: A case study of Dhungeta-Ramis sub-basin. *Ethiop. Geol. Ecol. Landsc.* **2020**, *5*, 65–80. [\[CrossRef\]](#)
56. Senthilkumar, M.; Gnanasundar, D.; Arumugam, R. Identifying groundwater recharge zones using remote sensing & GIS techniques in Amaravathi aquifer system, Tamil Nadu, South India. *Sustain. Environ. Res.* **2019**, *29*, 15.
57. Bera, A.; Mukhopadhyay, B.P.; Barua, S. Delineation of groundwater potential zones in Karha river basin, Maharashtra, India, using AHP and geospatial techniques. *Arab. J. Geosci.* **2020**, *13*, 693. [\[CrossRef\]](#)
58. Pourali, S.H.; Arrowsmith, C.; Chrisman, N.; Matkan, A.A.; Mitchell, D. Topography wetness index application in flood-risk-based land use planning. *Appl. Spat. Anal. Pol* **2016**, *9*, 39–54. [\[CrossRef\]](#)
59. Pourghasemi, H.R.; Beheshtirad, M. Assessment of a data-driven evidential belief function model and GIS for groundwater potential mapping in the Koohrang Watershed, Iran. *Geocarto Int.* **2014**, *30*, 662–685. [\[CrossRef\]](#)
60. Hasanuzzaman, M.D.; Mandal, M.H.; Hasnine, M.D.; Shit, P.K. Groundwater potential mapping using multi-criteria decision, bivariate statistic and machine learning algorithms: Evidence from Chota Nagpur Plateau, India. *Appl. Water Sci.* **2022**, *12*, 58. [\[CrossRef\]](#)
61. Cuthbert, M.O.; Acworth, R.I.; Andersen, M.S.; Larsen, J.R.; McCallum, A.M.; Rau, G.C.; Tellam, J.H. Understanding and quantifying focused, indirect groundwater recharge from ephemeral streams using water table fluctuations. *Water Resour. Res.* **2016**, *52*, 827–840. [\[CrossRef\]](#)
62. Golkarian, A.; Naghibi, S.A.; Kalantar, B.; Pradhan, B. Groundwater potential mapping using C5. 0, random forest, and multivariate adaptive regression spline models in GIS. *Environ. Monit. Assess.* **2018**, *190*, 149. [\[CrossRef\]](#)
63. Shaban, A.; Khawlie, M.; Abdallah, C. Use of Remote Sensing and GIS to Determine Recharge Potential Zones: The Case of Occidental Lebanon. *Hydrogeol. J.* **2006**, *14*, 433–443. [\[CrossRef\]](#)
64. Costache, R.; Hong, H.; Pham, Q.B. Comparative assessment of the flash-flood potential within small mountain catchments using bivariate statistics and their novel hybrid integration with machine learning models. *Sci. Total Environ.* **2020**, *711*, 134514. [\[CrossRef\]](#)
65. Abdelkareem, M.; El-Baz, F.; Askalany, M.; Akawy, A.; Ghoneim, E. Groundwater prospect map of Egypt's Qena Valley using data fusion. *Int. J. Image Data Fusion* **2012**, *3*, 169–189. [\[CrossRef\]](#)
66. Kebede, S. *Groundwater in Ethiopia: Features, Numbers and Opportunities*; Springer Hydrogeology: Berlin/Heidelberg, Germany, 2013. [\[CrossRef\]](#)
67. Opp, C. Bodenkörper. In *Geographie—Physische Geographie und Humangeographie*, 3rd ed.; Gebhardt, H., Glaser, R., Radtke, U., Reuber, P., Vött, A., Eds.; Springer: Berlin/Heidelberg, Germany, 2011; pp. 485–490.
68. Senanayake, I.P.; Dissanayake, D.M.D.O.K.; Mayadunna, B.B.; Weerasekera, W.L. An approach to delineate groundwater recharge potential sites in Ambalantota, Sri Lanka using GIS techniques. *Geosci. Front.* **2016**, *7*, 115–124. [\[CrossRef\]](#)
69. Shekhar, S.; Pandey, A.C. Delineation of groundwater potential zone in hard rock terrain of India using remote sensing, geographical information system (GIS) and analytic hierarchy process (AHP) techniques. *Geocarto Int.* **2015**, *30*, 402–421. [\[CrossRef\]](#)
70. Han, L.; Liu, Z.; Ning, Y.; Zhao, Z. Extraction and analysis of geological lineaments combining a DEM and remote sensing images from the northern Baoji loess area. *Adv. Space Res.* **2018**, *62*, 2480–2493. [\[CrossRef\]](#)
71. Abdelkareem, M.; El-Baz, F. Remote sensing of Paleodrainage systems west of the Nile River, Egypt. *J. Geocarto Int.* **2017**, *32*, 541–555. [\[CrossRef\]](#)
72. Obi Reddy, G.P. Evaluation of groundwater potential zones using remote sensing data—A case study of Gaimukh watershed, Bhanadra District, Maharastra. *J. Indian Soc. Remote Sens.* **2000**, *28*, 19–32. [\[CrossRef\]](#)
73. Pradeep, R. Remote sensing techniques to locate ground water potential zones in upper Urmil River Basin, District Chhatarpur—Central India. *J. Indian Soc. Remote Sens.* **1998**, *26*, 135–147.
74. Sreedhar, G. Mapping of groundwater potential zones in the Musi basin using remote sensing data and GIS. *Adv. Eng. Softw.* **2009**, *40*, 506–518.
75. Elewa, H.H.; Qaddah, A.A.; El-Feel, A.A. Determining potential sites for runoff water harvesting using remote sensing and geographic information systems-based modeling in Sinai. *Am. J. Environ. Sci.* **2012**, *8*, 42–55.
76. Zhu, Q.; Abdelkareem, M. Mapping groundwater potential zones using a knowledge-driven approach and GIS analysis. *Water* **2021**, *13*, 579. [\[CrossRef\]](#)



77. Krishna, R.; Kishan, D.; Sarup, J. Lineament extraction and lineament density assessment of Omkareshwar, M P, India, using GIS Techniques. *Int. J. Eng. Manag. Res.* **2015**, *5*, 717–720.
78. Singh, L.K.; Jha, M.K.; Chowdary, V.M. Assessing the accuracy of GIS-based MultiCriteria Decision Analysis approaches for mapping groundwater potential. *Ecol. Indic.* **2018**, *91*, 24–37. [[CrossRef](#)]
79. Hong, Y.; Abdelkareem, M. Integration of remote sensing and a GIS-based method for revealing prone areas to flood hazards and predicting optimum areas of groundwater resources. *Arab. J. Geosci.* **2022**, *15*, 114. [[CrossRef](#)]
80. Abdelkareem, M.; Abdalla, F.; Mohamed, S.Y.; El-Baz, F. Mapping paleohydrologic features in the arid areas of Saudi Arabia using remote sensing data. *Water* **2020**, *12*, 417. [[CrossRef](#)]
81. Lee, S.; Pradhan, B. Probabilistic landslide hazards and risk mapping on Penang Island, Malaysia. *J. Earth Syst. Sci.* **2006**, *115*, 661–672. [[CrossRef](#)]
82. Bamousa, A.O.; Matar, S.S.; Daoudi, M.; Al-Doaan, M.I. Structural and geomorphic features accommodating groundwater of Al-Madinah City, Saudi Arabia. *Arab. J. Geosci.* **2013**, *6*, 3127–3132. [[CrossRef](#)]
83. Howard, A.D. Drainage analysis in geologic interpretation: A summation. *AAPG Bull.* **1967**, *51*, 2246–2259.

**Disclaimer/Publisher’s Note:** The statements, opinions and data contained in all publications are solely those of the individual author(s) and contributor(s) and not of MDPI and/or the editor(s). MDPI and/or the editor(s) disclaim responsibility for any injury to people or property resulting from any ideas, methods, instructions or products referred to in the content.